**Proceedings of ASME Turbo Expo 2020**
**Turbomachinery Technical Conference and Exposition**
**GT2020**
**June 22-26, 2020, London, England**

**GT2020-15212**

# NONLINEAR RESPONSE AND STABILITY OF AN EXPERIMENTAL OVERHUNG COMPRESSOR MOUNTED WITH A SQUEEZE FILM DAMPER

**William J. Gooding[1], Matthew A. Meier[1], Edgar J. Gunter[2], and Nicole L. Key[1]**

[1]Purdue University, West Lafayette, IN, USA
[2]University of Virginia and RODYN Vibration Analysis, Charlottesville, VA, USA

## ABSTRACT

*This paper presents rotordynamic data obtained within a test facility studying the aerodynamics of a high-speed centrifugal compressor for aero-engine applications. The experimental overhung compressor is supported by two rolling element bearings. The compressor-end ball bearing is supported by an oil-fed squeeze film damper.*

*After some period of operation, the compressor began to exhibit a unique nonlinear increase in the rotordynamic response followed by an unexpected subsynchronous whirl instability as the speed continued to increase. Finally, as the rotor speed was increased further, the rotor re-stabilized.*

*A numerical model of the compressor system was created using a commercially available software suite. This model indicates the effective weight of the damper support has a significant effect on the frequency of the second critical speed. Increasing this weight causes the second critical speed, originally predicted at 35,200 RPM, to shift down to 15,650 RPM. This increase in the support weight is due to inertial interaction between the damper support and the surrounding static structure. The increased shaft deflection that occurs as the rotor passes through this shifted critical speed causes the damper to lockup, resulting in the increased response observed experimentally. At a slightly higher speed, Alford-type aerodynamic cross-coupling forces excite the two subsynchronous critical speeds. Finally, as the rotor departs from the second critical speed, the damper unlocks and is able to effectively suppress the Alford-type instabilities, allowing the rotor to return to stable operation.*

Keywords: rotordynamics, squeeze film damper, centrifugal compressor

## NOMENCLATURE

| | |
|---|---|
| CSTAR | Centrifugal Stage for Aerodynamic Research |
| $K_{ij}$ | Element of a stiffness matrix |

## INTRODUCTION

Aircraft engines typically contain multiple rolling element bearings mounted in oil-fed squeeze film dampers to facilitate stable operation well above the first critical speed. In these rotor-bearing systems, self-excited whirl motion can arise and be severe enough to cause catastrophic damage to the rotor system. Self-excited whirl refers to that motion which is excited by forces associated with the rotor motion itself. This is in contrast to unbalance (or other forced vibrations) in which the source of the excitation is present when the rotor is stationary [1]. Nonsynchronous whirling can be caused by many mechanisms including fluid-film bearing instability, internal friction, and aerodynamic cross-coupling. For stable operation, the system damping must be sufficient to suppress the instabilities arising from the various sources [2].

Aerodynamic cross-coupled forces of the Alford type arise in centrifugal compressor systems due to circumferential asymmetries in clearance gaps between rotating and stationary components. In labyrinth seals, circumferential variation in clearance leads to a corresponding variation in static pressure. This static pressure disparity leads to a periodic force within the seal, which lags the rotor displacement by an angle between 0 and 90 degrees. The magnitude and nature of this cross-coupling tends to be driven by seal geometry, seal pressure drop, and vibration frequency [3]. In unshrouded impellers and axial rotors, asymmetric tip clearances are caused by shaft non-concentricity or nonuniform blade heights. This leads to an uneven torque distribution around the circumference which can generate forward whirl [3]. These cross-coupled forces were

first described for axial-flow turbomachines, however, they have also been observed and studied in radial stages [4], [5].

Damping can be developed from many sources within the rotordynamic system. The most common approach for stabilizing rotors subject to strong instabilities is to incorporate a squeeze film damper support system to encase the bearing [2], [6]. However, the performance of such a support must be carefully tuned to effect an increase in system stability. A support with damping and stiffness values that deviate from optimum can result in a deterioration in performance relative to the baseline [2], [7], [8]. For short dampers (with small length-to-diameter ratios), the Reynolds Equation may be applied to compute stiffness and damping values [7], [9]. Squeeze film dampers exhibit highly nonlinear behavior and their performance is highly sensitive to damper clearance and rotor eccentricity [2], [7].

Significant work has been completed over the past decades to accurately characterize and predict the rotordynamic behavior of complex systems involving squeeze film dampers and strong aerodynamic cross-coupling. Many of these studies are focused on the analytic development of modelling capabilities [6], [10]–[12] or on experimental tests of simplified configurations [9], [13]–[16]. Various studies have been conducted on rocket engine turbopump systems operating without squeeze film dampers [17]–[19]. However, there are relatively few examples of rotordynamic data collected on realistic systems involving centrifugal impellers, labyrinth seals, and squeeze film dampers operating at high speeds [5], [8], [20].

This paper presents rotordynamic data obtained within a test facility studying the aerodynamics of a high-speed centrifugal compressor for aero-engine applications. These data allow observation of phenomena related to the interaction of aerodynamic cross-coupling and damper forces in a nonidealized application.

## EXPERIMENTAL FACILITY

The rotordynamic data presented in this paper were acquired in the Centrifugal Stage for Aerodynamic Research (CSTAR) facility at Purdue University. The system is driven by a 1,400 hp (1 MW) AC electric motor. A speed-increasing gearbox, with a gear ratio of 30.46, couples the electric motor to the compressor drive shaft. The CSTAR facility includes an auxiliary oil system designed to support the lubrication and cooling requirements of the compressor driveline and gearbox. Mobil Jet Oil II is supplied to the gearbox journal bearings, compressor rolling element bearings, and to the squeeze film damper. Ambient air is drawn through several screens to condition the flow upstream of the compressor inlet. The compressor mass flow rate is controlled via a throttle valve installed in the primary exhaust line routed to ambient. Full details of the research facility can be found in [21].

The rotating system is designed to operate at a corrected speed of 22,500 RPM resulting in mechanical design speeds between approximately 21,000 RPM and 23,500 RPM depending on ambient conditions. The impeller has 15 full and 15 splitter blades and is fixed to the shaft with two interference fits and a lock nut. The lightweight aluminum nosecone is mounted to the impeller with an interference fit and is bolted to the forward end of the shaft. The clearance between the impeller and the shroud is set using shims to shift the shroud axially. The backface cavity is sealed using two sets of labyrinth seals with three teeth. Bleed air is removed from the cavity downstream of the forward (larger diameter) seal through two independently throttled and measured offtake lines. A small amount of air is scavenged through the rear (smaller diameter) seal to prevent oil leakage into the flow path. The forward seal has a designed clearance of 0.0075” (0.19 mm) at a diameter of 6.927” (175.9 mm) while the rear seal has a designed clearance of 0.005” (0.13 mm) at a diameter of 1.778” (45.16 mm) and is maintained at a pressure drop of ~2 psi (13.8 kPa) during tests.

The shaft is supported by two bearings and torque is transmitted from the gearbox through a bellows-type flexible coupling with a spline interface. The rear bearing is a cylindrical roller bearing and the forward thrust bearing is an angular contact ball bearing, which is supported in a squeeze film damper. The damper was designed to have a clearance of 0.003” (0.08 mm) at a diameter of 5.12” (130 mm). The ends of the damper are sealed with O-rings spaced 0.947” (24.1 mm) apart, and oil is fed through a deep groove and a single weep hole is present to allow through-flow. The damper is supported by a squirrel cage flexible support with a spring rate of 200,000 lb/in (35,000 N/mm) that is pinned and fixed to the static structure. Four Bentley Nevada proximity probes are used to monitor the shaft orbit behavior—two each located 90 degrees apart at two axial locations, termed “Forward” and “Rear”. Circumferentially, the probes are located 45 degrees on either side of top-dead-center, where positive angles are measured opposite to impeller rotation. To maintain bearing life, steady operation above 0.001” (0.025 mm) of shaft deflection is not permitted. A detailed cross-section of the system is given in Figure 1. The system operated with adequate mechanical stability for several years, through various aerodynamic hardware iterations and compressor surge tests, but it has

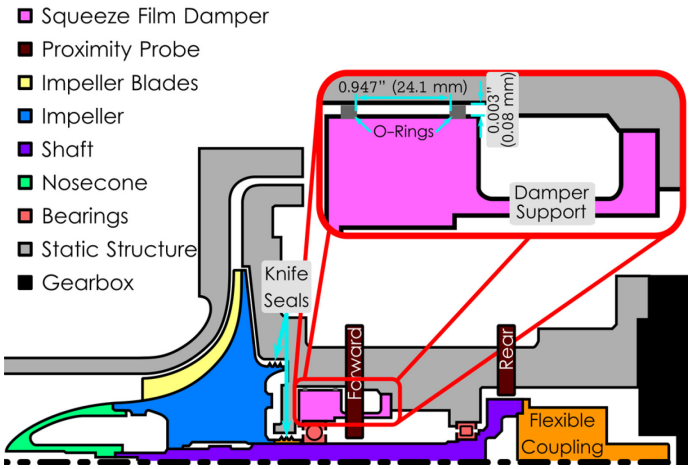


**FIGURE 1:** COMPRESSOR CROSS SECTION

recently begun exhibiting shaft deflections in excess of limits for a large portion of the operating speed range.

## NUMERICAL APPROACH

Computational analysis was performed using the *DyRoBeS* (Dynamics of Rotor Bearing Systems) software suite. This software is capable of linear and nonlinear computation of both free and forced vibration and of calculating steady and dynamic performance of bearings, including squeeze film dampers. The numerical model developed for this analysis is displayed graphically in Figure 2. The rotordynamic system is broken into a finite number of stations. The bearings are connected to a fixed foundation as "flexible supports" to include their stiffness and, when applicable, damping characteristics. The shaft, impeller, impeller blades, and the nosecone are portrayed in different colors corresponding to their different materials and densities.

Stations 1 through 15 represent the mass discretization locations of the shaft. The nosecone and impeller are computed as a separate rotor system with mass discretization locations indicated by Stations 16 through 21. The connection between the two rotor systems is modelled by three internal springs representing their physical interfaces. The internal spring at Station 6 is shown in Figure 2 while the others are hidden for clarity. Aerodynamic cross-coupling forces (for the nonlinear analyses) are applied at Station 18, as indicated by the forward-most "flexible support" in Figure 2, and unbalance is applied at Station 4, as indicated by the red triangle. For this analysis, 1 oz-in (72 g-cm) of unbalance was added to the compressor representing an approximately 0.001" (0.025 mm) offset between the installed impeller and shaft centerlines. Station 22 represents the interface between the squeeze film damper and the forward bearing.

Aerodynamic cross-coupling forces are implemented numerically as a linear constant bearing with zero diagonal components ($K_{xx}$ and $K_{yy}$) and the off-diagonal components

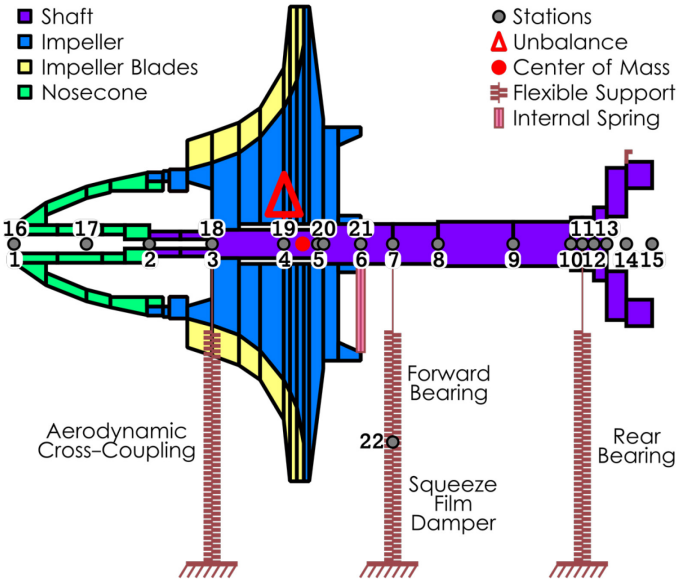


**FIGURE 2:** ANALYTICAL MODEL

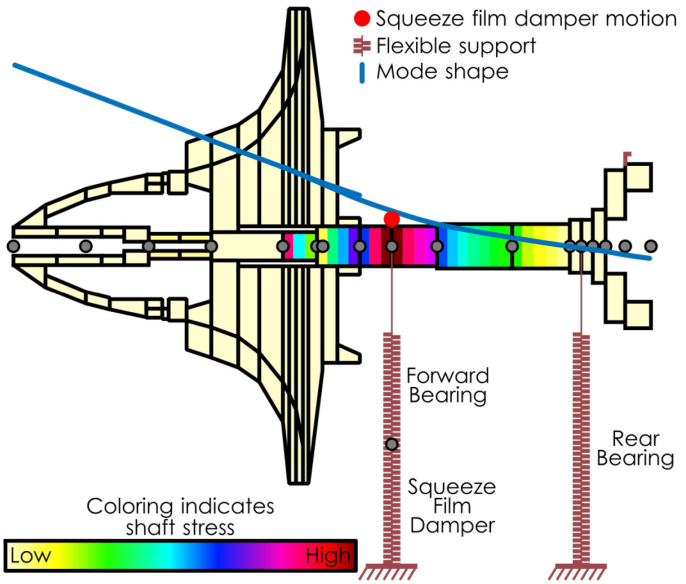


**FIGURE 3:** FIRST CRITICAL SPEED MODE SHAPE WITH ORIGINAL SUPPORT WEIGHT (5,659 RPM)

computed as suggested in [3]. In linear analyses, the squeeze film damper is treated as an isotropic bearing with prescribed stiffness and damping coefficients. In nonlinear analyses, the forces for the damper are computed from the Reynolds equation based on the damper geometry as described in [7].

This model was used to predict the first critical speed and corresponding mode shape of the system, Figure 3. This mode is predicted to occur at 5,659 RPM (94.3 Hz), which corresponds closely with what has been observed experimentally. In this conical mode, the compressor and damper are moving in phase with each other as indicated by the red circle (indicating the motion of the squeeze film damper) falling on the same side of the centerline as the impeller tip motion. Very little deflection is predicted at the rear bearing while the deflection increases going forward, as expected for an overhung rotor. The shaft stress reaches a maximum at the forward bearing location. The second mode is predicted to be at 35,200 RPM, well above the highest operating speed of the compressor. In this initial critical speed analysis, the cross-coupling forces were not included, and the weight of the squeeze film damper support structure was modelled accurately as 16 lb (71 N).

## EXPERIMENTAL RESULTS

Since 2015, the squeeze film damper has provided sufficient damping for stable operation throughout the entire operating speed range. However, recently the rotordynamic characteristics of the system changed. The peak deflection response for each of the four proximity probes for the full speed range is provided in Figure 4. Below 10,000 RPM, there are no discernible peaks in the response that surpass the limit levels of 0.001" (0.025 mm). The peak in response corresponding to the first critical speed occurs at 5,570 RPM (92.8 Hz), closely matching the prediction from the analytical model. The phase

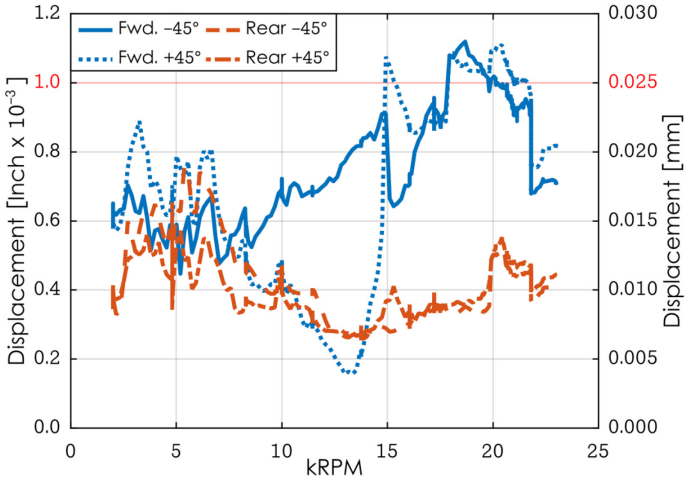


**FIGURE 4:** EXPERIMENTALLY DETERMINED 0-PEAK PROXIMITY PROBE RESPONSE THROUGH OPERATING RANGE

angle of the synchronous portion of the proximity probe signal is presented in Figure 5. This illustrates the gradual 180° phase shift in the response that occurs as the system passes through the first critical speed. Adequate damping is present at this point as indicated by the low level of response measured in passing through the critical speed. The squeeze film damper was designed to allow stable operation through the first critical speed. In that respect, the damper is behaving as intended. However, the behavior is not satisfactory at higher speeds.

The first observation of unexpected high-speed behavior occurred at approximately 15,000 RPM (250 Hz). As illustrated in Figure 4, the two Forward (Fwd.) proximity probes show a nonlinear increase in amplitude while the two Rear probes remained relatively unchanged. The deflection indicated by the Forward +45° probe increased by more than 80% of the limit value while the Forward -45° probe decreased by 25% of the limit value. Simultaneously, the Forward probes exhibit step changes in the phase angle of the response,

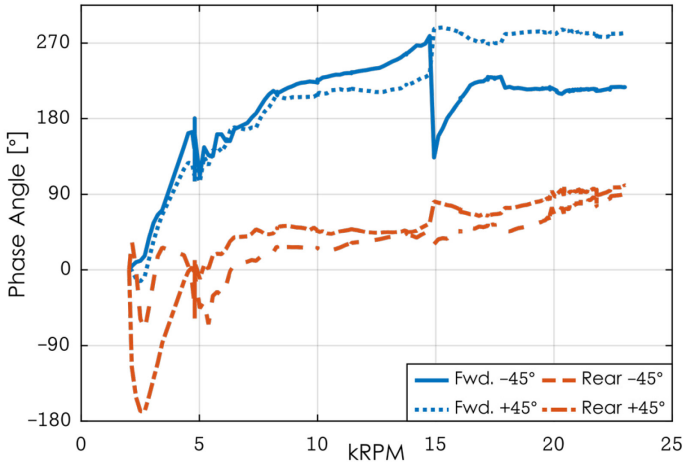


**FIGURE 5:** EXPERIMENTALLY DETERMINED PHASE ANGLE OF SYNCHRONOUS PORTION OF PROXIMITY PROBE SIGNALS THROUGH OPERATING RANGE

suggesting the system is passing through a resonant speed. This abrupt increase in amplitude is an indication of an overloaded damper operating at too high an eccentricity ratio. When a squeeze film damper orbits through a large fraction of the available clearance the damper stiffness rapidly approaches the stiffness of the bearing, known as damper lockup, and a step increase occurs in the rotor motion [7]. Waterfall plots showing the frequency content of the Forward probes' responses through this phenomenon are presented in Figure 6. The step change in the overall response is associated with a step change in the synchronous (1X) response at approximately 250 Hz—a step increase for the Forward +45° probe and a step decrease for the Forward -45° probe). A less-dramatic step increase is also apparent in both of the probes at twice the running frequency (2X) due to nonlinear effects within the rotordynamic system.

A second unexpected change in the response occurred at approximately 18,000 RPM. At this speed, the response of both Forward probes suddenly stepped above the limit criteria. The frequency content of this event is given in Figure 7. This step change in the overall response is accompanied by a step change in the frequency characteristics of the signal. A signal is present at 17,500 RPM that corresponds to ½ of the running engine frequency. At 18,000 RPM, the signal in both probes suddenly splits into two distinct bands at approximately 92.7 Hz (5,560 RPM) and at 210 Hz (12,600 RPM). These spectral peaks do not track with the rotor speed as it is increased (that is, they do not stay at a constant engine order), and there is no corresponding step change in the synchronous (1X) response.

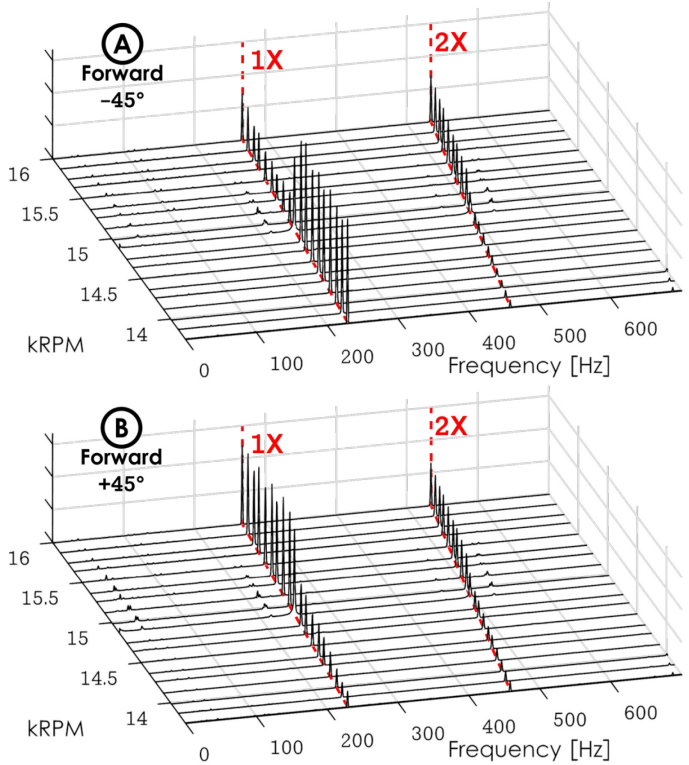


**FIGURE 6:** WATERFALL DIAGRAM OF STEP CHANGE IN RESPONSE AT 15,000 RPM, FORWARD -45° (A) AND +45° (B) PROXIMITY PROBES

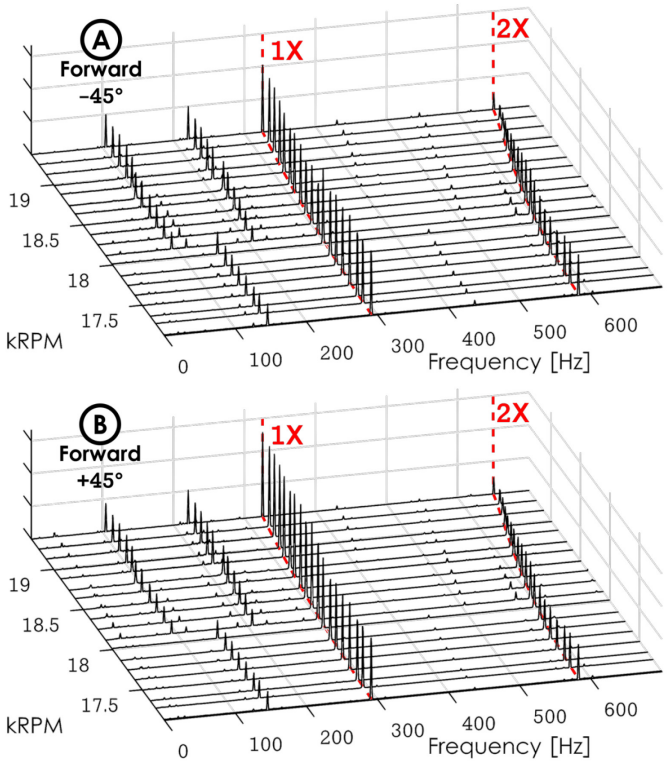


**FIGURE 7:** WATERFALL DIAGRAM OF SUBSYNCHRONOUS RESPONSE, 17,000 RPM TO 20,000 RPM, FORWARD -45° (A) AND +45° (B) PROXIMITY PROBES

This behavior—both in terms of deflection (Figure 4) and frequency content (Figure 7)—remained present until 21,500 RPM when the system stabilized and responses dropped below the safety limit.

This behavior can also be visualized by plotting the orbital motion of the shaft constructed from a pair of perpendicular proximity probes located at the same axial location. The orbits constructed using the Forward probes at 12,000 RPM (A), 18,000 RPM (B), and 21,800 RPM (C) are presented in Figure 8. The scale is consistent through the three orbits, data are plotted for a duration of 0.05 seconds, and the red dots indicate the beginning of a revolution referenced to a once-per-revolution pulse signal. The 12,000 RPM orbit demonstrates stable shaft whirl dominated by synchronous motion. The motion is elliptical due to either the presence of an asymmetric stiffness or asymmetric preload from gravitational forces or assembly effects. The orbit at 18,000 RPM shows unstable motion with strong subsynchronous precession. This subsynchronous motion is represented in the waterfall plot (Figure 7) by the two frequency peaks present below the engine operating frequency. The large amplitude in the orbit is problematic due to the strong forces transmitted through the bearings that are implied which may cause premature failure. Finally, the 21,800 RPM orbit indicates that at increased speeds the rotor system has returned to a stable whirl motion dominated by a synchronous signal.

## NUMERICAL RESULTS

These high-speed behaviors had not been observed previously and their origin was unknown. The numerical model was methodically manipulated to match the observed compressor response. Previous studies have shown the significant impact of support weight on the rotordynamic response of a flexible rotor [10]. Specifically, it was determined that an increase in the support weight can significantly decrease the second critical speed while not causing a discernible shift in the first critical speed for a simplified system. This behavior could explain the suspected modal response occurring in the test compressor at 15,000 RPM.

To investigate this, the weight of the damper support was artificially increased in the numerical model to a value of 150 lb (667 N). This artificially high weight for the support may be attributed to the interaction of the casing and support structure with the damper. Once damper lockup occurs, the inertia of the surrounding casing system may be influencing the motion of the system and causing the damper to act as if it had a

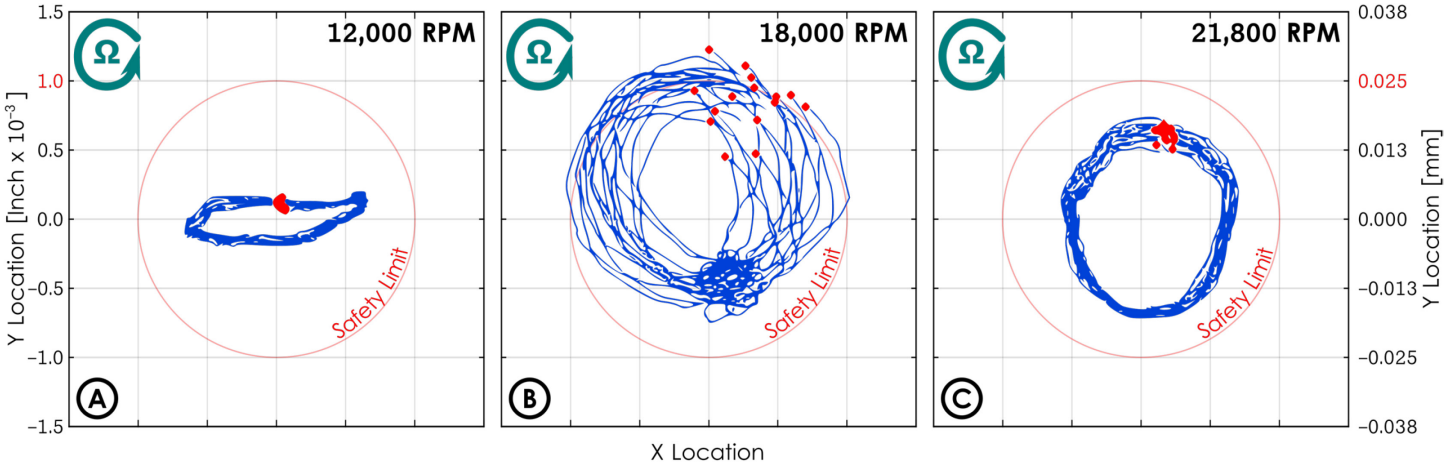


**FIGURE 8:** EXPERIMENTAL ORBIT CHARACTERISTIC AT FORWARD PROBE LOCATION AT 12,000 RPM (A), 18,000 RPM (B), AND 21,800 RPM (C)

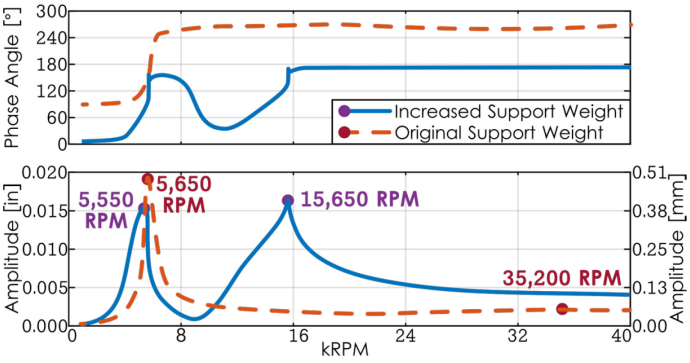


**FIGURE 9:** PREDICTED RESPONSE AT STATION 1 WITH INCREASED AND ORIGINAL SUPPORT WEIGHTS

significantly higher effective weight.

The predicted amplitude and the phase of the response at Station 1 with the increased damper weight and the original damper weight is presented in Figure 9. This linear analysis did not include the effects of aerodynamic cross-coupling. The corresponding mode shapes for both support weights are displayed in Figure 10. As evident, the increased damper weight has caused the second critical speed to shift from 35,200 RPM down to 15,650 RPM, nearly matching the experimental measurements without significantly shifting the first critical speed. This conical mode is referred to as a bifurcated first critical speed in which the compressor mode shape resembles the first mode except that the damper support housing is moving out of phase with the impeller, as indicated by the orange circle and the predicted motion of the impeller tip falling on opposite sides of the shaft centerline in Figure 10. This is a bifurcated first mode (rather than a pure second mode) based on the effect of support mass on rotordynamic response presented in [10] and the experimental data. The frequency at which this mode occurs is highly sensitive to the assumed

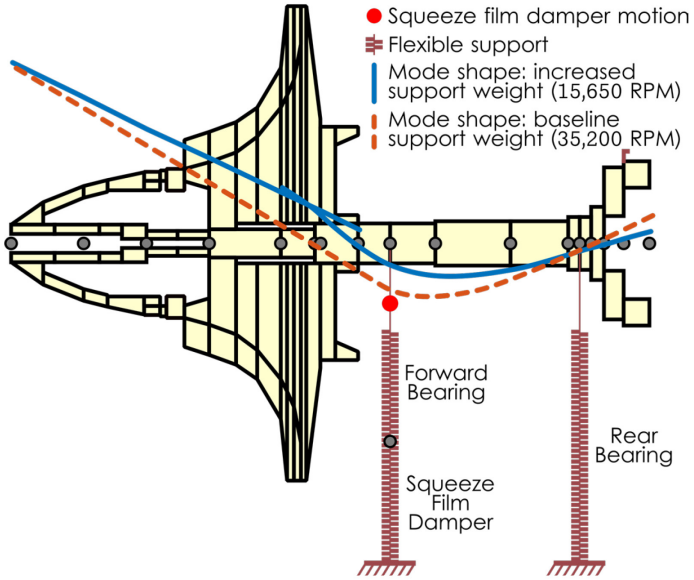


**FIGURE 10:** SECOND MODE SHAPE WITH INCREASED SUPPORT WEIGHT (15,650 RPM) AND ORIGINAL SUPPORT WEIGHT (35,200 RPM)

weight of the supporting structure. In other words, the critical speed is likely to shift depending upon the degree of inertial interaction between the spring support and the surrounding structure. Increased support effective weight causes the mode to shift to lower frequencies. This would suggest that an increase in the damper motion, causing greater inertial interaction with the surrounding structure, nonlinearly decreases the expected second critical frequency.

To further investigate the dynamics of the system at this second critical speed, a nonlinear time-transient analysis of the rotor motion at a constant speed of 15,650 RPM was conducted. In the time-transient analysis, the rotor equations of motion are integrated forward in time and the squeeze film forces on the bearing are calculated from the integration of the fluid-film pressure profile based on the Reynolds Equation. Gravity, unbalance, and aerodynamic cross-coupling were all considered in this analysis. The motion is computed over approximately 40 cycles of shaft motion with 1,000 time steps per cycle. The method of computation chosen was the Wilson-Theta method due to experience in obtaining good convergence with the method for similar applications.

The results of the nonlinear time-transient analysis are presented in Figure 11. These results indicate that the rotor is unstable with significant nonsynchronous whirling with the increased support weight (Figure 11A). Limit cycle motion occurs due to nonlinear forces in the squeeze film damper placing an upper bound on the growth of the orbital motion. For the same transient analysis, the motion of the shaft within the damper bearing (Station 22 in Figure 2) is illustrated in Figure 12 with the red circles indicating the beginning of each rotor revolution. Limit cycle motion is exhibited at 67% of the available clearance. The damping and stiffness of squeeze film dampers is known to increase rapidly above an eccentricity ratio of 0.4, resulting in a drastic rise in the forces transmitted through the damper [7]. The transient analysis predicts a maximum of greater than 1500 lb (6.7 kN) of force transmitted through the damper through this critical speed. These high forces are likely to cause damage to the damper and bearing if allowed to persist for a significant length of time. The transient analysis predicts stable operation with the original support weight as indicated in Figure 11B.

## Connection to Experimental Phenomena

Alford-type aerodynamic cross-coupling forces combine with the increased damper support weight to manifest the large, limit-cycle motion predicted in this second mode and the experimentally observed phenomena; specifically, the unexpected excessive response between 15,000 and 21,500 RPM. The inertial interaction between the damper support and the surrounding structure causes the second critical speed to shift to a significantly lower speed than originally expected. While the second critical speed was designed to fall far above the maximum design speed of the stage, the increased effective support weight shifts it into the operating regime. Experimentally, this mode is excited at 15,000 RPM and is responsible for the concomitant step changes in shaft deflection

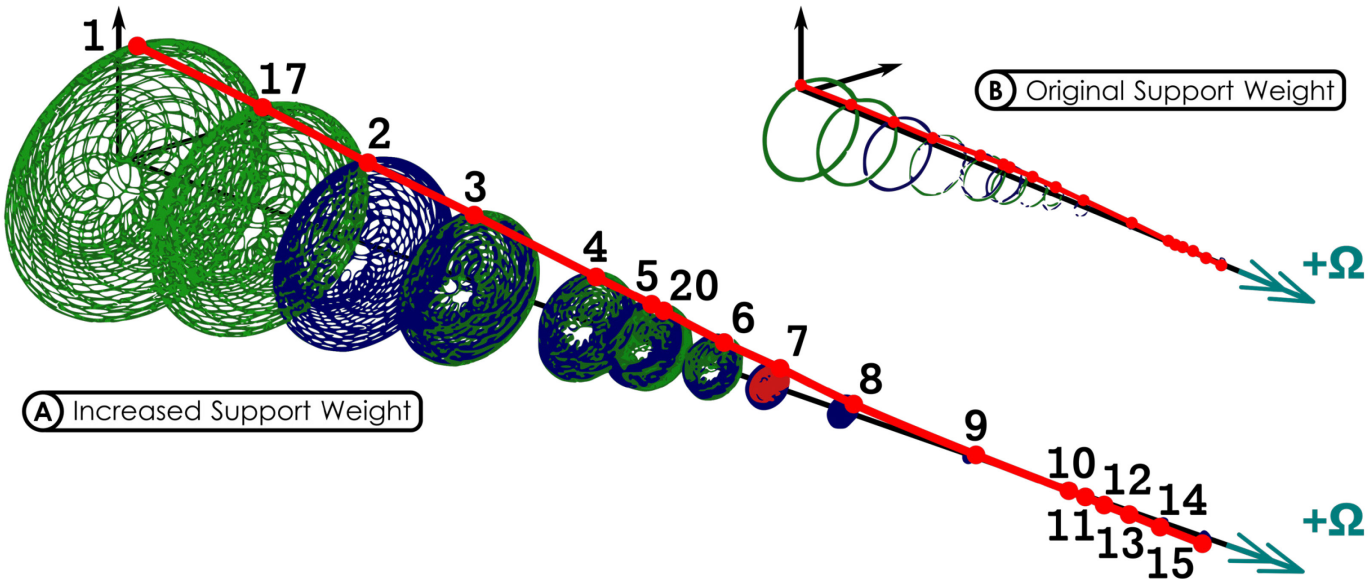


**FIGURE 11:** NONLINEAR TIME TRANSIENT COMPRESSOR MOTION AT 15,650 RPM WITH INCREASED SUPPORT WEIGHT (150 LB, 667 N) (A) AND THE ORIGINAL SUPPORT WEIGHT (16 LB, 71 N) (B)

magnitude (Figure 4), phase angle (Figure 5), and frequency spectra (Figure 6) that were observed. Depicted in Figure 9, the numerical model predicts this second critical speed to be broad; that is, it will generate a significant response for a relatively wide range of frequencies. The nearly instantaneous increase in the experimental response indicates that damper lockup has occurred. As the rotational speed of the compressor is further increased in passing through this modal frequency, the damper remains locked, providing very little damping, as the energy in the system continues to increase.

The frequency content of the transient compressor motion at the forward bearing location (station 7) is presented in Figure 13. This indicates that the limit cycle motion displayed in Figure 11 is dominated by half-order (0.5X) and synchronous (1X) with additional low-frequency motion and response at 1.5 and 2 times synchronous (1.5X and 2X). The experimental data indicate primarily 1X and 2X response between 15,000 and 18,000 RPM with additional content at 0.5X and 1.5X (low-level) arising between 16,500 and 18,000 RPM. This difference could arise due to the experimental operation at non-constant speed. The rotor is accelerated through this speed region to avoid operating at steady state in this dangerous region whereas the computational analysis assumes prolonged operation at a constant rotational speed.

The increased effective support weight is sufficient for explaining the experimental data around 15,000 RPM; however, the measured response at 18,000 RPM arises only due to the interaction of the Alford-type aerodynamic cross-coupling forces and the inertial interaction between the damper support and the surrounding structure. Additional energy enters the system as the rotor speed is increased which, because the damper remains locked, increases the degree of inertial interaction. This causes a nonlinear decrease in the second critical speed of the system below the speed at which it was first observed. With the reduced effectiveness of the damper, the aerodynamic cross-coupling excites the two

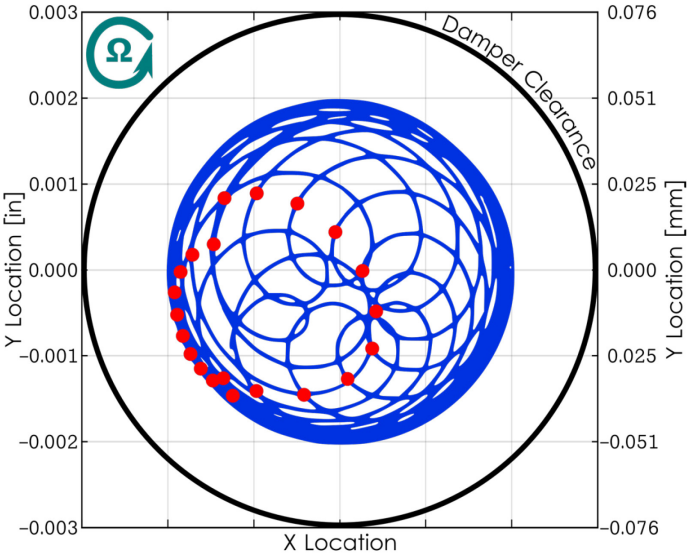


**FIGURE 12:** MOTION OF SHAFT IN DAMPER BEARING (STATION 22) AT 15,650 RPM WITH INCREASED SUPPORT WEIGHT

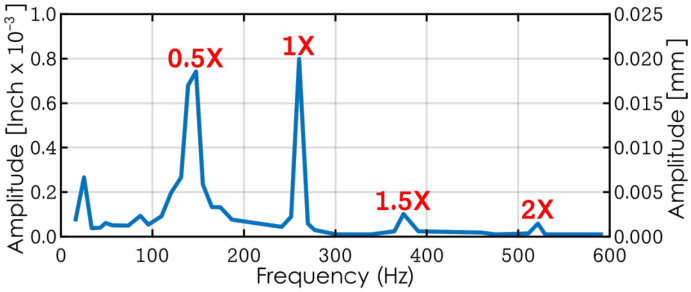


**FIGURE 13:** FFT OF RESPONSE AT STATION 7 FROM TIME TRANSIENT COMPUTATION AT 15,650 RPM

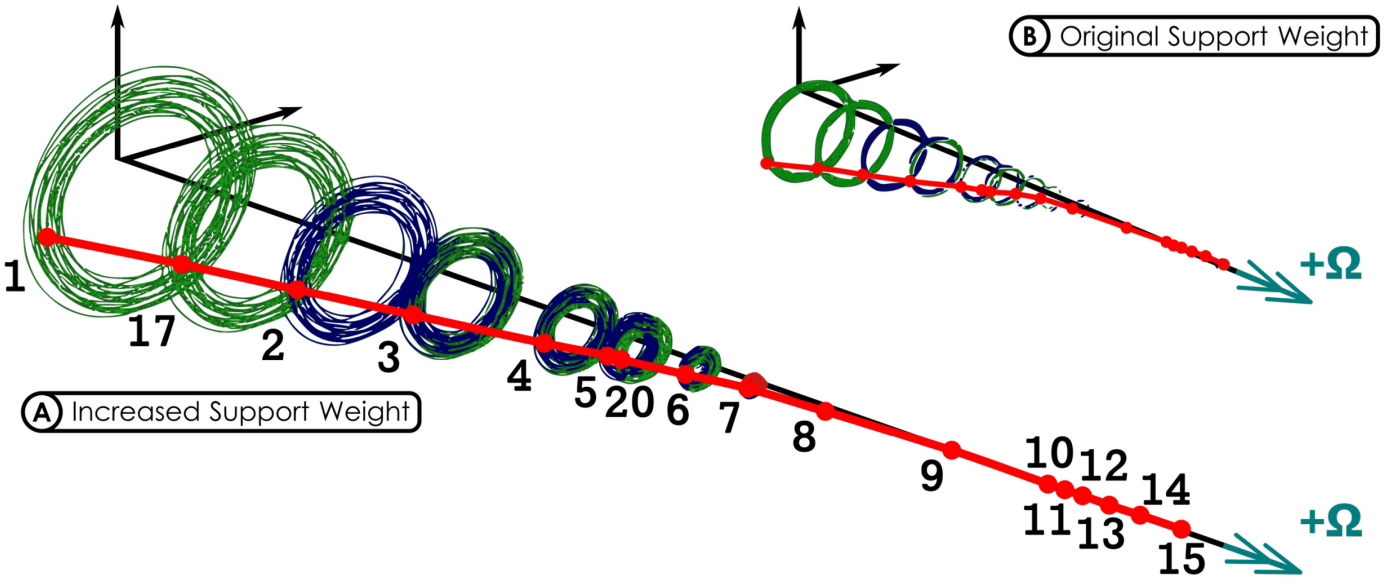


**FIGURE 14:** NONLINEAR TIME TRANSIENT COMPRESSOR MOTION AT 24,000 RPM SHOWING STABLE SYNCHRONOUS MOTION OF THE SYSTEM WITH INCREASED SUPPORT WEIGHT (150 LB, 667 N) (A) AND THE ORIGINAL SUPPORT WEIGHT (16 LB, 71 N) (B)

subsynchronous critical speeds that are present in the evolving system. The excitement of these two subsynchronous critical speeds is indicated in the waterfall plot (Figure 7) by the two spectral peaks at 92.7 Hz (5,560 RPM) and at 210 Hz (12,600 RPM). Because these subsynchronous frequencies are excited by the Alford-type forces, the synchronous response will not be affected. This matches the spectral response observed experimentally (Figure 7). Thus, the combination of aerodynamic cross-coupling forces and an increase in the effective weight of the damper support produce the unexpected rotordynamic characteristic of the experimental system.

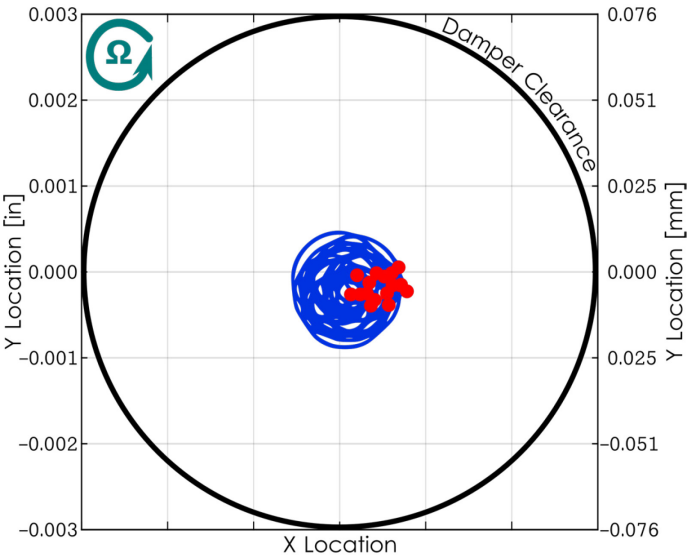


**FIGURE 15:** MOTION OF SHAFT IN DAMPER BEARING (STATION 22) AT 24,000 RPM WITH INCREASED SUPPORT WEIGHT

## Return to Stability

Typically, systems that exhibit strong, unstable, nonsynchronous whirl motion due to Alford forces do not return to stability at higher speeds [2]. This system, however, was able to operate with stable precession beyond the unstable region. The numerical model accurately predicts the return to stability that was indicated experimentally. A nonlinear time-transient simulation was conducted at a speed of 24,000 RPM using the same approach described previously. The transient motion of the shaft is indicated in Figure 14, and the motion of the damper is presented in Figure 15. The shaft, as a whole, exhibits stable, synchronous motion at this speed for both support weights while the damper displays stable, low-level motion without significant whirl. This return to stability arises due to the nonlinear behavior of the damper. As the operating speed departs further from the broad second critical speed, the damper is no longer locked up. Once unlocked, the damper is able to once again provide sufficient damping to suppress the Alford-type self-excited whirl. This eliminates the presence of the strong subsynchronous whirl and permits the rotor to return to stable operation at the higher speeds.

## Root Cause Analysis

This analysis has provided valuable insight into the physical mechanisms driving the unique rotordynamic characteristics observed on the test compressor. However, the numerical model cannot explain the root cause of the change in behavior. The compressor operated in a stable manner within these speed ranges through several years of testing before exhibiting the behavior described in this work. Several possible causes could lead to the shift in behavior. After the current aerodynamic test campaign is complete, the rotating system will be disassembled and fully inspected to determine which source is the primary driver.

The most likely source is the degradation of the sealing O-rings installed in the squeeze film damper. This degradation would lead to leakage from the damper landing and would alter the rotordynamic characteristics of the system. The effective length of the damper would be reduced leading to a decrease in the damper's stiffness and damping. Additionally, an O-ring failure could impede proper centering of the damper which would increase the propensity of lockup to occur. Furthermore, the damper's characteristic is extremely sensitive to clearance. If any debris from a degraded O-ring were to remain within the damper the performance would shift significantly. This debris could provide the physical mechanism for the inertial interaction suggested by the numerical analysis. Together, these factors could result in the observed behavior.

Other sources include the rubbing of abradable surfaces, pilot erosion, and bearing wear. Both knife seals and the impeller shroud include abradable coatings to prevent damage to critical hardware in the event of rotor-stator contact. Over time, this coating could erode slightly resulting in increased asymmetry in the clearances and an increase in the magnitude of Alford forces. Erosion of pilot surfaces used in mating the impeller to the shaft could lead to an increased offset between the center of mass of the impeller and the center of rotation of the shaft. Wear in the bearings due to a recent test campaign with many compressor surge events could increase the eccentricity of the shaft rotation within the bearing. Both of these could increase the load on the damper, increase the inertial interaction between the damper support and the surrounding structure, and lead to the behavior observed.

## CONCLUSION

Regardless of the precise origin of the behavior, these data represent a unique observation of a complex rotordynamic system. The authors have observed similar behavior in operational equipment; however, this is the first publication on the topic (to the authors' knowledge) due to typical proprietary restrictions. These effects are likely to only be observed in real-world applications where non-ideal drivers exist.

This paper presents rotordynamic data portraying an unexpected shift in the response of a single-stage centrifugal compressor supported by two rolling element bearings, one of which is mounted in a squeeze film damper. Unexpected high-speed behavior was observed in excess of operational safety limits. A numerical model of the system was developed and matched to the experimental data yielding valuable insight into the drivers of the unique behavior:

- Inertial interaction between the damper support and the surrounding structure lead to an increased effective damper weight and decreased predicted speed of the second mode from 35,200 to 15,650 RPM.
- This mode is extremely sensitive to the degree of interaction and the resulting effective mass of the damper support
- The large motion associated with this mode results in damper lockup, drastically decreasing the damping in the system
- This reduced damping allows Alford-type aerodynamic cross-coupling instabilities to excite two subsynchronous critical speeds as the experimental rotor operates between 18,000 and 21,500 RPM.
- With a further increase in speed, the excitation due to the second critical speed is reduced allowing the damper to unlock. The damping is then sufficient to suppress the Alford instabilities and return the system to stable operation.

Future work will focus on the determination of the root cause of the shift in behavior as mentioned previously. Furthermore, additional instrumentation will be pursued to better characterize the response of the system including the transient clearance on the knife seals, the motion of the tip of the nosecone, and the motion of the damper support itself. These data will allow greater insight into the dynamics of the system. With this added instrumentation, it is desirable to further investigate and precisely record the behavior of the squeeze film damper under various levels of unbalance and installed damper clearance.

## ACKNOWLEDGEMENTS

The authors would like to thank Rolls-Royce Corporation for its funding and permission to publish this work. They would also like to acknowledge Grant Malicoat for his extensive support of the test campaign associated with this work.

## REFERENCES


[1] R. G. Kirk, A. A. Alsaeed, and E. J. Gunter, "Stability Analysis of a High Speed Automotive Turbocharger," in *Proceedings of IJTC2006*, 2006, pp. 1–8.

[2] E. J. Gunter, "Rotor-Bearing Stability," in *Proc. of the First Turbomachinery Symposium*, 1972, pp. 119–141.

[3] J. S. Alford, "Protecting Turbomachinery From Self-Excited Rotor Whirl," *J. Eng. Power*, vol. 87, no. 4, pp. 333–343, 1965.

[4] A. H. Lerche, G. O. Musgrove, J. J. Moore, C. D. Kulhanek, and G. Nordwall, "Rotordynamic Force Prediction of an Unshrouded Radial Inflow Turbine Using Computational Fluid Dynamics," *Proc. ASME Turbo Expo*, vol. 7 A, pp. 1–6, 2013.

[5] R. G. Kirk, "Evaluation of Aerodynamic Instability Mechanisms for Centrifugal Compressors-Part I: Current Theory," *J. Vib. Acoust.*, vol. 110, no. 2, pp. 201–206, 1988.

[6] W. J. Chen, M. Rajan, S. D. Rajan, and H. D. Nelson, "The Optimal Design of Squeeze Film Dampers for Flexible Rotor Systems," *J. Mech. Transm. Autom. Des.*, vol. 110, no. 2, pp. 166–174, 1988.

[7] E. J. Gunter, L. E. Barrett, and P. E. Allaire, "Design of Nonlinear Squeeze-Film Dampers for Aircraft Engines," *J. Lubr. Technol.*, vol. 99, no. 1, pp. 57–64, 1977.

[8] E. J. Gunter, L. E. Barrett, and P. E. Allaire, "Stabilization of Turbomachinery with Squeeze Film Dampers - Theory and Applications.," in *Institution of Mechanical Engineers*, 1976, pp. 1–10.

[9] E. J. Gunter and M. P. Proctor, "Whirl Motion of a Seal Test Rig with Squeeze-Film Dampers," in *Vibration Institute 31st Annual Meeting*, 2007, pp. 1–12.

[10] R. G. Kirk and E. J. Gunter, "Effect of Support Flexibility and Damping on the Dynamic Response of a Single Mass Flexible Rotor in Elastic Bearings.," *J. Eng. Ind.*, pp. 221–232, 1972.

[11] W. J. Chen, "Instability threshold and stability boundaries of rotor-bearing systems," *J. Eng. Gas Turbines Power*, vol. 118, no. 1, pp. 115–121, 1996.

[12] E. J. Gunter and W. J. Chen, "Dynamic Analysis of an 1150 MW Turbine-Generator," in *Proceedings of the ASME Power Conference*, 2005, pp. 1–9.

[13] D. L. Ransom, J. Li, L. A. San Andrés, and J. Vance, "Experimental Force Coefficients for a Two-Bladed Labyrinth Seal and a Four-Pocket Damper Seal," *J. Tribol.*, vol. 121, no. 2, pp. 370–376, 1999.

[14] O. C. De Santiago and L. A. San Andrés, "Imbalance Response and Damping Force Coefficients of a Rotor Supported on End Sealed Integral Squeeze Film Dampers," *J. Eng. Gas Turbines Power*, vol. 121, pp. 718–724, 1999.

[15] L. A. San Andrés and O. C. De Santiago, "Imbalance Response of a Rotor Supported on Flexure Pivot Tilting Pad Journal Bearings in Series with Integral Squeeze Film Dampers," *J. Eng. Gas Turbines Power*, vol. 125, no. 4, pp. 1026–1032, 2003.

[16] M. P. Proctor and E. J. Gunter, "Stability Analysis of a High-Speed Seal Test Rotor With Marginal and Extended Squeeze-Film Dampers — Theoretical and Experimental Results," TM-2007-214849, 2007.

[17] E. J. Gunter and R. D. Flack, "Experimental Measurements of the Space Shuttle Main Engine Fuel and Oxygen Turbopump Vibration Characteristics," in *International Instrumentation Symposium*, 1981, p. 22.

[18] E. J. Gunter, "Dynamic Characteristics and Stability Analysis of Space Shuttle Main Engine Oxygen Pump," in *60th Shock and Vibration Symposium*, 1989, pp. 1–30.

[19] K. Yada, M. Uchiumi, and K. Funazaki, "Thomas/Alford Force on a Partial-Admission Turbine for the Rocket Engine Turbopump," *J. Fluids Eng.*, vol. 141, no. 1, pp. 1–9, 2019.

[20] R. G. Kirk, "Evaluation of Aerodynamic Instability Mechanisms for Centrifugal Compressors - Part II: Advanced Analysis," *J. Vib. Acoust.*, vol. 110, no. 2, pp. 201–206, 1988.

[21] C. J. Methel, W. J. Gooding, J. C. Fabian, N. L. Key, and M. Whitlock, "The Development of a Low Specific Speed Centrifugal Compressor Research Facility," in *ASME Turbo Expo*, 2016, pp. 1–11.